DR. PHILIP M BEART (Orcid ID : 0000-0002-7604-4558)



Article type : Original Article

# Inhibition of bioenergetics provides novel insights into recruitment of PINK1-dependent neuronal mitophagy

Yea Seul Shin[1,2,3], James G. Ryall[4], Joanne M. Britto[1], Chew L. Lau[1], Rodney J. Devenish[5], Phillip Nagley[5*], Philip M. Beart[1,6*†]

[1] Florey Institute of Neuroscience and Mental Health, Parkville, VIC 3052, Australia

[2] Department of Anatomy & Neuroscience, University of Melbourne, Parkville, VIC 3052, Australia

[3] Current address: Department of Microbiology, Infection and Immunity Program, Biomedicine Discovery Institute, Monash University, Clayton, VIC 3800, Australia

[4] Department of Physiology, University of Melbourne, Parkville, VIC 3052, Australia

[5] Department of Biochemistry and Molecular Biology, Monash University, Clayton VIC 3800, Australia

[6] Department of Pharmacology, University of Melbourne, Parkville, VIC 3052, Australia

* These authors contributed equally to this work

†Corresponding author. Florey Institute of Neuroscience and Mental Health, University of Melbourne, Parkville, Victoria 3010, Australia. Tel.: +61 3 8344 7324; fax: +61 3 9035 3107

E-mail address: phil.beart@florey.edu.au (P.M. Beart)

**Abstract**

Contributions of damaged mitochondria to neuropathologies have stimulated interest in mitophagy. We investigated triggers of neuronal mitophagy by disruption of mitochondrial energy metabolism in primary neurons. Mitophagy was examined in cultured murine cerebellar granule cells after inhibition of mitochondrial respiratory chain by drugs rotenone, 3-nitropropionic acid, antimycin A and potassium cyanide, targeting complexes I, II, III and IV, respectively. Inhibitor concentrations producing slow cellular demise were determined from analyses of cellular viability, morphology of neuritic damage, plasma membrane permeability and oxidative phosphorylation. Live cell imaging of dissipation of mitochondrial membrane potential ($\Delta\Psi_m$) by drugs targeting mitochondrial complexes was referenced to complete depolarization by CCCP. While inhibition of complexes I, III and IV effected rapid dissipation of $\Delta\Psi_m$, inhibition of complex II using 3-nitropropionic acid led to minimal depolarization of mitochondria. Nonetheless, all respiratory chain inhibitors triggered mitophagy as indicated by increased aggregation of mitochondrially localized PINK1. Mitophagy was further analyzed using a dual fluorescent protein biosensor reporting mitochondrial relocation to acidic lysosomal environment. Significant acidification of mitochondria was observed in neurons treated with rotenone or 3-nitropropionic acid, revealing mitophagy at distal processes. Neurons treated with antimycin A or cyanide failed to show mitochondrial acidification. Minor dissipation of $\Delta\Psi_m$ by 3-nitropropionic acid coupled with vigorous triggering of mitophagy suggested depolarization of mitochondria is not a necessary condition to trigger mitophagy. Moreover, weak elicitation of mitophagy by antimycin A, subsequent to loss of $\Delta\Psi_m$, suggested that mitochondrial depolarization is not a sufficient condition for triggering robust neuronal mitophagy. Our findings provide new insight into complexities of mitophagic clearance of neuronal mitochondria.

**Key words** Bioenergetics . Depolarization . Lysosome . Mitophagy . Neuron . PINK1 .

**Abbreviations**

| | |
|---|---|
| 3-NP | 3-nitropropionic acid |
| AA | Antimycin A |
| CCCP | Carbonyl cyanide m-chlorophenyl hydrazone |
| CGCs | Cerebellar granule cells |
| DMSO | Dimethyl sulfoxide |
| ECAR | Extracellular acidification rate |
| FCCP | Carbonyl cyanide 4-(trifluoromethoxy)phenylhydrazone |
| IMM | Inner mitochondrial membrane |
| KCN | Potassium cyanide |
| MEM | Minimum essential medium |
| MPT | Mitochondrial permeability transition |

| | |
|---|---|
| MTT | 3-(4,5-dimethylthiazol-2-yl)-2,5-diphenyltetrazolium bromide |
| OCR | Oxygen consumption rate |
| OMM | Outer mitochondrial membrane |
| OXPHOS | Oxidative phosphorylation |
| PBS | Phosphate buffered saline |
| PI | Propidium iodide |
| Rot | Rotenone |
| RRID | Research Resource Identifiers |
| SDHA | Succinate dehydrogenase complex, subunit A |
| TMRM | Tetramethylrhodamine methyl ester |
| XF | Extracelluar Flux |

**Introduction**

Neurons are metabolically active cells that have high energy demand for special functions. These cells rely strongly on mitochondrial oxidative phosphorylation to meet their ATP requirements, which are essential for synaptic function, involving release and reuptake of neurotransmitters, intracellular transport, and generation of action potentials. Dysfunction of mitochondria has been widely recognized as a key biochemical feature of neurodegenerative diseases (Beal 2005, Chaturvedi & Beal 2013, Golpich *et al.* 2017) and the failure to clear damaged mitochondria contributes to neurodegenerative processes (Baker *et al.* 2014, Chen & Chan 2009). The intracellular roles of mitochondria are not only to produce ATP but also to regulate ionic distribution, particularly that of $Ca^{2+}$ (Kann & Kovacs 2007), and to act as a trigger for cell death mechanisms (Smith *et al.* 2008). Therefore, quality control of mitochondria, through selective removal of damaged or dysfunctional organelles, is essential for overall neuronal function. Mitophagy is a major mitochondrial quality control process (Lemasters 2005, Youle & Narendra 2011, Ashrafi & Schwarz 2013), by which dysfunctional mitochondria are specifically triggered for destruction through the general autophagic machinery leading to their degradation in lysosomes (Baker *et al.* 2014).

At the outset, depolarization of mitochondria was recognized as a trigger of mitophagy (Narendra *et al.* 2008). Therefore, in many studies on the biochemical mechanisms of mitophagy in cultured mammalian cells, the uncoupling agent, carbonyl cyanide m-chlorophenyl hydrazone (CCCP) has been used to dissipate the electrical membrane potential ($\Delta\Psi_m$) across the inner mitochondrial membrane (IMM). Such dissipation of the $\Delta\Psi_m$ arrests the mitochondrial import of full length PINK1 leading to its accumulation at the outer mitochondrial membrane (OMM) (Geisler *et al.* 2010, Matsuda *et al.* 2010, Narendra *et al.* 2010, Vives-Bauza *et al.* 2010) on which PINK1 undergoes dimerization, activation and autophosphorylation (Kondapalli *et al.* 2012, Okatsu *et al.* 2012, Okatsu *et al.* 2013). Activated PINK1 initiates mitophagy by phosphorylating ubiquitin and recruitment of the E3 ubiquitin ligase Parkin on the OMM (Narendra *et al.* 2010, Jin *et al.* 2010,

Kane *et al.* 2014). Parkin causes ubiquitin chains to polymerize on OMM proteins (Sarraf *et al.* 2013), triggering a feed-forward mechanism (Ordureau *et al.* 2014). The multimeric phospho-ubiquitin chains on mitochondria recruit autophagy receptors to initiate autophagosome formation and trigger delivery of the damaged mitochondria to the acidified lysosomes via the autophagic pathway (Lazarou *et al.* 2015, Bingol & Sheng 2016, Sekine & Youle 2018).

Mitophagy has been observed in a range of cellular systems, including yeast and cultured mammalian cells. Factors that are considered as potential triggers of mitophagy (in addition to depolarization of mitochondria) include starvation, oxidative stress, reduced glutathione levels, fragmentation of mitochondria and the onset of the mitochondrial permeability transition (MPT) (Elmore *et al.* 2001, Rodriguez-Enriquez *et al.* 2004, Priault *et al.* 2005, Kim *et al.* 2007, Kanki & Klionsky 2008, Twig *et al.* 2008, Van Laar *et al.* 2015). Since each of these factors could themselves engender depolarization of mitochondria, we considered that a more focused study of the disruption of mitochondrial energy metabolism in the elicitation of mitophagy would be incisive. Such insights would be especially useful in the context of the specialized roles of neurons and their reliance on mitochondria in light of abundant evidence that mitochondrial dysfunction contributes to various neurological conditions (Beal 2005, Chaturvedi & Beal 2013, Golpich *et al.* 2017).

Accordingly, we carried out a systematic disruption of the mitochondrial respiratory chain in cultured primary neurons (murine cerebellar granule cells (CGCs)), by employing a set of pharmacological agents each of which inhibits a specific respiratory enzyme complex (Scheffler 2011): rotenone (Rot), complex I; 3-nitropropionic acid (3-NP), complex II; antimycin A (AA), complex III; potassium cyanide (KCN), complex IV. We also employed CCCP that chemically depolarizes mitochondria, to eliminate $\Delta\Psi_m$. Mitophagy was studied both by localization of PINK1 to mitochondria, and by use of a biosensor based on fluorescent protein technology, which reports the relocation of mitochondria to an acidic environment (namely, that of the lysosome). We found that while elicitation of vigorous mitophagy occurred under the inhibition of complex II by 3-NP, this agent failed to strongly depolarize mitochondria. Depolarization of mitochondria is therefore not a necessary condition for mitophagy in these neurons. On the other hand, the strong mitochondrial depolarization effected by the other agents used here did not always trigger by vigorous mitophagy, indicating that depolarization may not even be a sufficient condition for eliciting mitophagy.

## Materials and methods

### Materials

Neurobasal™ medium (Cat# 21103049), $Ca^{2+}$-, $Mg^{2+}$-free Hanks' Balanced Salt Solution (Cat# 14170112), B-27 supplement (Cat# 17504044), L-glutamine (Cat# 25030081), penicillin/streptomycin (Cat# 15140122), qualified fetal bovine serum, HEPES buffered salt solution (Cat# 15630080), Lipofectamine 2000 (Cat# 11668019), Opti-MEM I (reduced serum medium; Cat#31985070), minimal essential medium (MEM; Cat# 11095080), MEM without phenol red (Cat# 51200038), sterile NUNC cell culture plates, tetramethylrhodamine methyl ester perchlorate (TMRM; Cat# T668), Hoechst 33342 (Cat# H3570) were purchased from Thermo Fisher Scientific (Melbourne, Australia). Potassium chloride (KCl; Cat# P5405), poly-D-lysine (Cat# P0899), $MgSO_4.7H_2O$ (Cat# M2773), Trypsin from porcine pancreas (Cat# T4799),

deoxyribonuclease I from bovine pancreas (DNase I; Cat# D5025), sodium pyruvate (Cat# S8636), bovine serum albumin lyophilized powder (Cat# A9418), aphidicolin (Cat# A0781), dimethyl sulfoxide (DMSO; Cat# D8418), 3-(4,5-dimethylthiazol-2-yl)-2,5-diphenyltetrazolium bromide (MTT; Cat# M5655), propidium iodide (PI; Cat# P4170), paraformaldehyde (Cat# P6148), carbonyl cyanide 3-chlorophenylhydrazone (CCCP; Cat# C2759), rotenone (Rot; Cat# R8875), 3-nitropropionic acid (3-NP; Cat# N5636), antimycin A (AA; Cat# A8674) and potassium cyanide (KCN; Cat# 60178) were purchased from Sigma-Aldrich (Sydney, Australia). Mouse monoclonal primary antibody against succinate dehydrogenase complex, subunit A (Anti-SDHA; Abcam Cat# ab14715, RRID:AB_301433), goat anti-mouse IgG H&L (Alexa Fluor® 488) (Abcam Cat# ab150113, RRID:AB_2576208) and goat anti-rabbit IgG H&L (Alexa Fluor® 488) (Abcam Cat# ab150077, RRID:AB_2630356) secondary antibodies were purchased from Abcam (USA). For the measurement of mitochondrial respiration using Seahorse XF24 analyzer, Seahorse XF24 Mito Stress Assay (Cat# 103015-100) and XF24 V7 Cell Culture Microplates (24 wells) were purchased from Seahorse Bioscience (North Billerica, MA). Carbonyl cyanide 4-(trifluoromethoxy)phenylhydrazone (FCCP; Cat# C2920) and oligomycin (Cat# 75351) were purchased from Sigma-Aldrich (Sydney, Australia). Swiss White mice (MGI Cat# 5306408, RRID:MGI:5306408), were purchased from Animal Resources Centre, Canning Vale, WA, Australia; pregnant females were shipped at 13 days *post-coitus*.

**Cell culture**

Animal handling was carried out according to the guidelines of the National Health and Medical Research Council (NHMRC, Australia) and received institutional ethical approval (#13-084) from the Florey Institute of Neuroscience and Mental Health. Primary cultures of murine cerebellar granular cells (CGCs) were established from the cerebella of Swiss White mice (postnatal day 6-8, mouse pups of both sexes) as previously described (Giardina *et al.* 1998, Diwakarla *et al.* 2009). Mouse pups were decapitated, and their brains were placed in petri dishes containing ice-cold isolating buffer (Hanks' Balanced Salt Solution pH 7.4 containing 3 mg/ml BSA, 1.16 mM $MgSO_4$, 1 mM sodium pyruvate, 10 mM HEPES, 7.6 mM D-glucose) in which cerebella were dissected. Meninges from isolated cerebella were carefully removed and cerebella were chemically and mechanically dissociated in the presence of 0.2 % trypsin, 80 µg/ml DNase and centrifuged. Cells were resuspended in growth medium (Neurobasal™ medium, B-27 supplement (2 % v/v), 25 mM KCl, 500 µM L-glutamine, 100 U/ml penicillin-streptomycin) containing 10 % fetal bovine serum. Cells were plated in multi-well plates pre-coated with poly-D-lysine (50 µg/mL) and were maintained in a humidified incubator with reduced oxygen atmosphere (5% $CO_2$, 8.5% $O_2$ with balance of gases in $N_2$, 37°C). CGCs were exposed to 10% fetal calf serum for the first 24 h *in vitro* (Cheung *et al.* 1998) and full medium change was performed at 1 day *in vitro* with growth medium containing aphidicolin (1 µg/ml) to restrain non-neuronal cell proliferation (Diwakarla *et al.* 2009, Giardina *et al.* 1998). Half medium changes were conducted at 4 days *in vitro* and all experiments were performed at 7 days *in vitro*. These cultures were routinely found to contain > 95% of neurons that are immunopositive for neuronal marker, microtubule-associated protein-2 characteristic of neuronal phenotype, with a minimum number of non-neuronal cells (data not shown) (Cheung *et al.* 1998, Moldrich *et al.* 2001).

**Drug treatment**

CGCs were treated with the following drugs, all obtained from Sigma Aldrich (Sydney, Australia): Rot, 3-NP, AA, KCN and CCCP. Stock solutions of each of Rot, AA and CCCP were prepared in dimethyl sulfoxide (DMSO), while KCN was dissolved in purified sterile water. Stocks of 3-NP were made by dissolving in a sufficient volume of 100 mM NaOH to yield a neutral solution (confirmed to be pH 7). All drugs were freshly prepared for each experiment. Serial dilutions of stock solutions of drugs were made in minimum essential medium (MEM) containing 25 mM KCl, and drugs were equilibrated for 1 h at 37°C in a humidified incubator with reduced oxygen as above. The final concentrations of DMSO in the treatment media were kept to 0.03-0.2% (Mercer *et al.* 2005). On the day of experiment at 7 days *in vitro* (i.e. 6 days after transfer to serum-free medium), growth medium in which CGCs had been cultured was replaced by MEM (25 mM KCl) and all drugs were added to the CGCs at the desired concentration. Control cells not exposed to drugs were also subjected to a similar complete medium change, including appropriate amounts of the DMSO vehicle, where relevant.

**Assessment of viability and cellular integrity**

Cell viability assays were carried out using the 3-(4,5-dimethylthiazol-2-yl)-2,5-diphenyltetrazolium bromide (MTT) reduction assay for overall metabolic function, as previously described (Cheung *et al.* 1998). CGCs were grown in 96-well plates at a density of 0.12 x $10^6$ cells/well. Cells were exposed to drugs for 24 h in an arbitrary pattern on a plate to avoid possible regional bias effects. MTT (0.5 mg/ml) was directly added to the original culture medium at the time of cessation of drug treatment. Cells were incubated in the humidified 37°C incubator for 30 min. The culture medium was completely aspirated and DMSO was added to dissolve formazan crystals. The absorbance was measured at 570 nm. Raw MTT data were standardized against cells incubated in 0.1% TX-100 (100% cell death) and expressed as percentage of vehicle control values (defined as 0% cell death). Assays were performed with n = 3-4 replicates in 3-4 independent experiments. Cells were also tested for uptake of propidium iodide (PI) as a measure of integrity of the plasma membrane, as previously described (Beart *et al.* 2007, Diwakarla *et al.* 2009, Higgins *et al.* 2009). Cultures were grown in 48-well plates (0.2 x $10^6$ cells/well) and exposed to drugs for 1, 4, 8 and 24 h. After drug treatment, cells were incubated with PI (10 µg/ml) and Hoechst 33342 (5 µg/ml) for 10 min. Cells were washed with pre-warmed phosphate buffered saline (PBS; 137 mM NaCl, 50 mM $Na_2HPO_4$, 50 mM $NaH_2PO_4$, pH 7.4) to remove unbound dye and immediately fixed with PBS containing 4 % paraformaldehyde (pH 7.4) for 10 min at room temperature. Images from arbitrarily selected fields (10-15 images, total number of cells 250-500) were taken using an Olympus IX71 inverted fluorescence microscope (535/617 nm for PI, 350/461 nm for Hoechst), connected to an Olympus c-5050 digital camera. Cells stained with PI and Hoechst were counted and the proportion of dead cells was expressed as the percentage of PI-stained cells over the total number of cells stained by Hoechst.

**Immunocytochemistry for PINK1 visualization**

All procedures for immunocytochemistry were as previously described (Lim *et al.* 2007, Diwakarla *et al.* 2009, Mercer *et al.* 2017). Briefly, CGCs were cultured on 13 mm round glass coverslips pre-coated with poly-D-lysine (50 µg/ml) in 24 well plates (0.35 x $10^6$ cells/well). Cells were fixed with 4% paraformaldehyde for 10 min at room temperature subsequent to drug treatment. After sample permeabilization (0.3% Triton X-100),

coverslips were treated with PBS containing 1% bovine serum albumin and incubated with the relevant primary antibody overnight at 4°C, followed by incubation with fluorescently labelled secondary antibody. PBS was used for all washing steps. Cells were incubated with anti-rabbit PINK1 antibody (3 μg/ml) (gift from Dr Janetta Culvenor, Department of Pathology, University of Melbourne) (George *et al.* 2010), followed by secondary antibody incubation (goat anti-rabbit antibody conjugated to Alexa 488; 1:200 dilution). Hoechst 33342 stain (5 μg/ml) was used to counterstain cell nuclei. Images from arbitrarily selected fields were taken with an Olympus IX71 inverted fluorescence microscope, connected to an Olympus C-5050 digital camera. For quantitative analyses, patterns of PINK1 immunolabelling were scored across arbitrarily selected fields of photomicrographs which were taken before the hypothesis of two patterns (diffuse and aggregated) of PINK1 labelling was postulated *post hoc* by an independent observer. Neurons were assigned to three distinct populations: cells showing diffuse distribution of PINK1, cells manifesting aggregating labelling, and dying cells exhibiting very weak PINK1 labelling. Analyses were performed on raw counts which were then expressed as a percentage of the total population of cells counted; typically, 250-500 cells were scored in each of duplicate wells per experimental condition. Data represent the mean ± SEM of two independent experiments. Two-way ANOVA was carried out, followed by Bonferroni's *post hoc* test. A P value $< 0.05$ was considered statistically significant.

Double immunolabelling was performed to detect complex II and PINK1. For the former, anti-SDHA mouse monoclonal antibody (1:100 dilution) was used to detect mitochondrial complex II, applying the secondary antibody goat anti-mouse Alexa 488 (1:200 dilution). PINK1 primary antibody was used as above (3 μg/ml), applying the secondary antibody goat anti-rabbit Alexa 568 (1:200 dilution). Hoechst 33342 stain (5 μg/ml) was used to counterstain cell nuclei. Samples were imaged by fluorescence laser scanning confocal microscopy using an Olympus FluoView 1000 inverted confocal microscope (Olympus, Japan).

**Live confocal imaging for mitochondrial polarization**

Mitochondrial polarization was monitored using tetramethylrhodamine methyl ester (TMRM) as previously described (Beart *et al.* 2007). CGCs cultured on 6-well plates ($2 \times 10^6$ cells/well) were initially washed twice with MEM without phenol red, containing KCl (25 mM). Prior to drug treatment, cells were loaded with TMRM (150 nM) for 15 min at 37°C and medium in each well was replaced by fresh medium containing drugs supplemented with TMRM (50 nM). Live cell imaging was carried out over specified time periods with parallel vehicle. To induce complete depolarization of mitochondria, the protonophore CCCP (10 μM) was added to cells (Minamikawa *et al.* 1999, Lim *et al.* 2001). Cells were kept at 37°C in dark at all times during treatment with TMRM. TMRM-labeled live neurons were analyzed using an inverted confocal microscope (Zeiss LSM 510 Pascal, Carl Zeiss, Oberkochen, Germany) fitted with 37°C, 5% $CO_2$ humidified stage incubator; images were captured at 543 nm with a 40x lens. The mean fluorescence intensities across populations of vehicle control and treated neurons were obtained by using LSM 5 Image Browser provided by Zeiss. Three fields of the well were arbitrarily imaged by a blinded observer, and the fluorescence intensity of each image was divided by the total number of neurons present in the imaging field. Each treatment group involved the imaging of at least 120 neurons in each of duplicate wells. Values were expressed as the mean ± SEM and are from n=3 independent experiments.

**Measurement of mitochondrial respiration with Seahorse XF24 analyzer**

Measurements of the oxygen consumption rate (OCR) and extracellular acidification rate (ECAR) in adherent intact primary neuronal cultures were performed using a Seahorse Extracelluar Flux (XF) XF24 Analyzer (Seahorse Bioscience, North Billerica, MA) (Ryall 2017). XF24 V7 Cell Culture Microplates (24 wells) (Seahorse Bioscience) were pre-coated with poly-D-lysine (50 μg/ml) onto which were plated neurons at a density of 100,000/well. Cells were maintained under standard culturing conditions and experiments were performed at 7 days *in vitro*. Neurons were exposed to MEM (with 25 mM KCl) (control) or MEM (with 25 mM KCl) containing Rot, 3-NP, AA or KCN, with full medium changes with unbuffered serum-free Seahorse assay medium (Seahorse Bioscience) containing KCl (25 mM), after 4 h and 24 h incubation. The plates were transferred to the Seahorse XF24 analyzer for subsequent analyses of OCR and ECAR. On the day before the planned experiment, XF24 Sensor Cartridges were left to hydrate overnight in XF24 Calibrant pH 7.4 solution (Seahorse Bioscience) at 37°C without $CO_2$. The instrument was left on overnight to stabilize at 37°C. On the day of experiment, cells were rinsed by adding 1 ml of warm unbuffered Seahorse assay medium and the plate was left in a 37°C incubator without $CO_2$ for 60 min as a de-gassing procedure before being loaded in the XF24 instrument for OCR/ECAR measurements. The OCR and ECAR were measured basally and after the sequential addition of four metabolic reagents, oligomycin, carbonyl cyanide 4-(trifluoromethoxy)phenylhydrazone (FCCP), Rot and AA, which were loaded into four ports of the sensor cartridge and injected sequentially into the cells. All Seahorse experiments were performed once as a blinded experiment; respiration and acidification rates are presented as the mean ± SEM (n = 3-5 wells per treatment group). Statistically significant differences between treatment groups were identified using one-way ANOVA with Bonferroni *post hoc* test.

**Monitoring mitophagy using the mt-Rosella biosensor**

mt-Rosella is a chimeric protein containing a pH-stable red fluorescent protein (DsRed.T4) linked to a pH-sensitive green fluorescent protein (pHlourin), the fusion protein being targeted to the mitochondrial matrix (Rosado *et al.* 2008, Mijaljica *et al.* 2011). At 6 days *in vitro*, CGCs (24 well plates; 0.35 x $10^6$ cells/well) were transfected with mt-Rosella plasmid using Lipofectamine 2000 Transfection Reagent (ThermoFisher Scientific, Melbourne) according to the manufacturer's instruction. Following transfection, cells were kept in reduced oxygen incubator for 24 h. Drug treatment with appropriate vehicle controls was carried out as above. Subsequent to drug treatment, direct fluorescence images of transfected neurons were captured with Olympus IX71 inverted fluorescence microscope, connected to an Olympus C-5050 digital camera. Fluorescence images were captured at 508 nm and 587 nm, to obtain green and red fluorescence, respectively.

The integrated intensity of green and red fluorescence, from selected fields corresponding to individual neurons, was quantified using ImageJ software (http://rsb.info.nih.gov.ij). The images were converted into 8-bit pictures and appropriate threshold was applied consistently in all fields under analysis. Raw values of integrated intensity of green and red fluorescence from 17-43 neurons (same number of fields) per experimental condition were aggregated over 4 replicate wells. The pooled data were normalized to the green/red integrated intensity ratios for parallel control untreated cells. Such normalized data were expressed

as mean ± SEM from two independent experiments in quadruplicate wells in each experiment. $P < 0.05$ was considered statistically significant based on unpaired *t*-test.

**Data Analysis**

Data are given as a mean ± SEM of the numbers of independent experiments as indicated. Comparative data sets were analyzed using one-way ANOVA (intra-group) or two-way ANOVA (comparing different populations), followed by Bonferroni's *post hoc* test. Sample sizes for the studies were not predetermined by statistical methods. Statistical analyses, normality of data (D'Agostino & Pearson normality test) and outlier test were undertaken using GraphPad Prism v. 4.0 (San Diego, CA, USA).

**Results**

**Determination of bioenergetic impairment induced by respiratory complex inhibitors**

To determine the appropriate concentrations of drugs to disrupt mitochondrial energy metabolism, CGCs were exposed for 24 h to varying concentrations of inhibitors to each of the respiratory complexes I, II, III and IV (Rot, 3-NP, AA and KCN, respectively). Concentrations chosen were based upon analyses of multiple indices of neuronal integrity, and took account of observations of drug-induced (i) damage to neuritic networks and its temporal dependence, (ii) cell viability employing the MTT assay, and (iii) patterns of PI labelling. The MTT assay allowed determination of the potencies of the respiratory complex inhibitors and the inhibitory concentration of each drug at 50% potency ($IC_{50}$) was obtained from cell viability curves. CGGs displayed concentration-dependent decreases in cell viability with all respiratory complex inhibitors (Supplementary Fig. 1). Here, like the two other strategies employed, there was some day-to-day variability, and notably with KCN. In conjunction with the morphological observations using phase contrast microscopy (data not shown), which focused upon progressive thinning of neuritic networks and cellular shrinkage, a suitable pair of concentrations, defined as “low” and “high” (Table 1), was selected to take account of the differential observations arising from the three indices of neuronal integrity. Inhibitor concentrations could therefore be chosen producing significant impairment of cellular function with slow cellular demise, distinct from necrotic-like injury, as judged by relatively low extents of plasma membrane permeabilization based on uptake of PI (Supplementary Fig. 2).

To characterize the impairment in bioenergetics caused by each of the respiratory complex inhibitors, CGCs were exposed to low and high concentrations of drugs for 4 h and 24 h; at each time the OCR was assessed using a Seahorse XF24 Extracellular Flux Analyzer (Supplementary Fig. 3). Overall, both basal oxygen consumption and FCCP-induced maximal respiratory capacity were reduced in CGCs exposed to low and high concentrations of Rot or 3-NP after 4 h and 24 h (Supplementary Fig. 3b-e). Exposure to high concentrations of AA (Supplementary Fig. 3f, g) and KCN (Supplementary Fig. 3d, e) also resulted in significant reduction in basal oxygen consumption and FCCP-induced maximal respiratory capacity, whereas the lower concentration in each case caused minimal disruption to bioenergetic indices (Supplementary Fig. 3).

In order to compare the bioenergetic status of neurons in all conditions, the relative basal OCR values were co-plotted with the ECAR to generate XF PhenoGrams (Fig. 1). In the theoretical case (Fig. 1a), arbitrary lines

were drawn to depict each of four possible basal bioenergetic states of CGCs: glycolytic, oxidative, high metabolism and low metabolism, represented as one of four quadrants, respectively (Ryall 2017). In general, drug treatment resulted in decreases in OCR levels, indicating loss of respiratory functions in CGCs. In some cases, a slight increase in ECAR was observed, likely in compensation for impaired oxidative phosphorylation (OXPHOS) (Fig. 1b-e). CGCs exposed to a prolonged treatment with low concentrations of Rot and 3-NP fell into the low metabolism quadrant (Fig. 1d), while cells treated with low concentrations of AA and KCN remained in the oxidative quadrant (Fig. 1b and d). The high concentrations of all drugs effectively shifted the metabolic state of cells towards the low metabolism state after 4 h treatment (Fig. 1c), which became more pronounced after 24 h exposure (Fig. 1e).

**Mitochondrial depolarization accompanying inhibition of the mitochondrial respiratory complexes**

The loss of $\Delta\Psi_m$ in neurons under treatment of respiratory complex inhibitors was examined using live cell confocal imaging, by monitoring the retention of TMRM fluorescence within mitochondria. Control neurons showed bright red TMRM fluorescence, with threads of mitochondria clearly visible in neuritic networks in each cell, particularly in the cytoplasm around the nucleus that was manifested as a clear void (Fig. 2a (top row)). TMRM fluorescence was rapidly and substantially reduced following treatment with CCCP (Fig. 2a, as expected for complete depolarization of mitochondria. The fluorescence intensity values from CCCP-treated neurons were taken as background intensity; for cells treated with other drugs, the adjusted values were expressed as a percentage of corrected control that was designated as 100% (Fig. 2b). TMRM fluorescence in CGCs treated with Rot and KCN displayed a rapid decrease in fluorescence as early as 0.5 h and 1 h down to less than 10% of control levels ($P < 0.0001$) (Fig. 2a, b), while depolarization induced by AA was slower, becoming significantly reduced after 1 h ($P < 0.05$) (Fig. 2b). However, treatment with 3-NP resulted in barely discernible reduction in TMRM fluorescence over the first hour of drug treatment and, while reduced after 4 h, was not significantly depressed (Fig. 2a, b). Overall, these results indicate that Rot and KCN caused the most significant depolarization of mitochondria, with AA less effective. By contrast, 3-NP had only a mild effect over the time-course of treatment, without significant change in $\Delta\Psi_m$.

**Distribution patterns of PINK1 reflecting mitophagy in CGCs under mitochondrial respiratory complex inhibition**

PINK1 is a primary initiator of mitophagy in mammalian cells, becoming stabilized on the OMM of mitochondria upon depolarization of the mitochondrial membrane (Narendra *et al.* 2008, Matsuda *et al.* 2010, Narendra *et al.* 2010). To analyze PINK1 retention on mitochondria subsequent to bioenergetic impairment, CGCs were treated with respiratory complex inhibitors for 4 h and the intracellular distribution of PINK1 was monitored using immunocytochemical staining with a PINK1-specific antibody. The majority of untreated control neurons display diffuse staining of PINK1 across the whole cell body (including the nuclear region) (Fig. 3a; Untreated control panel; yellow arrows). The enlarged images in Fig. 3b (upper row) indicates a cell with the “diffuse” morphology (Di). However, a small proportion of cells showed concentrated localization of PINK1 mainly in the cytosol, leaving the nuclear areas (stained with Hoechst 33342 dye) as a clear void (Fig. 3a; Untreated control panel; white arrow); this pattern of labeling is termed “aggregated” staining of PINK1. The enlarged images in Fig. 3b (lower row) indicates cells with the “aggregated” morphology (Ag). In CGCs

exposed to respiratory complex inhibitors, the aggregated pattern of PINK1 staining became more prominent quantitatively, such that a relatively higher proportion of PINK1 immunostaining was in the aggregated morphology (Fig. 3a; white arrows). This cytoplasmic aggregation of PINK1 surrounding nuclei in drug-treated cells corresponds to its localization to mitochondria: the immunofluorescence of PINK1 co-localizes substantially with that of mitochondrial respiratory complex II (see examples in Supplementary Fig. 4).

Compared to control, CGCs treated with Rot or 3-NP showed an increased proportion of cells showing aggregated PINK1 staining (control, 40% of population as opposed to Rot, 56% and 3-NP, 59%; $P < 0.0001$ in each case), while a significantly reduced proportion of CGCs displayed diffuse PINK1 staining (Fig. 3c). This redistribution, although smaller in magnitude, was also seen in CGCs exposed to AA or KCN where the proportion of cells showing aggregated PINK1 staining significantly increased (control, 31% as opposed to AA, 40% and KCN, 46%; $P < 0.0001$ in each case) (Fig. 3d). Likewise, there was a mild but significant reduction in the proportion of cells showing diffuse PINK1 staining (Fig. 3d). Overall, exposure to inhibitors of respiratory complexes I-IV induced PINK1 localization to mitochondria in CGCs.

**Determination of mitophagy with fluorescent mt-Rosella biosensor to monitor acidification of mitochondria**

In order to monitor the later stage of mitophagy during which mitochondria are relocated to an acidic environment, CGCs were transiently transfected with mt-Rosella and exposed to the respiratory complex inhibitors. Transfection with mt-Rosella enables the red fluorescence of its DsRed.T4 component to report the intracellular distribution of mitochondria. The quenching of green fluorescence of the pHluorin component reports delivery of those mitochondria into low-pH lysosomes (Rosado *et al.* 2008, Mijaljica *et al.* 2011, Sargsyan *et al.* 2015).

Untreated control CGCs transfected with mt-Rosella exhibited dual-labelled red (DsRed.T4) and green (pHluorin) fluorescence throughout the cell, indicative of a wide distribution of mitochondria in all compartments of a neuron, including the cell body, dendritic and axonal processes (Fig. 4a; Control panels). After exposure to respiratory complex inhibitors for 24 h, strong red fluorescence from mt-Rosella was displayed throughout the cell (Fig. 4a). In general, the overall cell morphology revealed some retraction of cellular processes (Fig. 4a). Treatment with Rot or 3-NP resulted in a notable overall reduction of green fluorescence. In the neuronal processes of treated cells, increased punctate distribution of both red and residual green fluorescence was observed, relative to untreated control neurons. However, regions within the cell body retained bright green fluorescence after cellular exposure to Rot or 3-NP (Fig. 4a). By contrast, in cells treated with AA, KCN or CCCP, the green and red fluorescence of mt-Rosella generally remained relatively bright throughout the cells (Fig. 4a). In these cases, there was a tendency to display punctate fluorescence in the distal regions relative to untreated control neurons.

Fluorescence intensities within individual neurons, expressed as the green/red fluorescence ratio, were quantified using ImageJ software. Because drug-treated neurons retained strong red and green fluorescence in the cell body area (see above), this quantitative analysis focused on the distal ends of neuronal processes. Any changes in green fluorescence in areas of the neuronal arbor could thus be quantified as the ratio of green fluorescence with respect to the intensity of red fluorescence (Fig. 4b). The green/red ratio from each drug-

treated neuronal population is presented as percentages of the ratio measured in control CGCs (designated as 100%). By this analysis, neurons exposed to Rot and 3-NP showed significant reductions in green/red ratio of mt-Rosella in neuronal processes compared to control (Rot, 72%, $P < 0.05$; 3-NP, 68% of control, $P < 0.01$, respectively), indicative of acidification of mitochondria in the distal parts of neurons (Fig. 4b). On the other hand, CGCs treated with AA and KCN did not show significant reduction in green fluorescence compared to control. Strikingly, after treatment of CGCs with CCCP, the green fluorescence in mt-Rosella transfected neurons actually increased (Fig. 4b). This phenomenon is due to the generalized collapse of proton gradients across intracellular membranes effected by CCCP, representing lack of acidification of lysosomes (even though mitophagy may have indeed directed mitochondria to that location). The nullification of intracellular locational reporting by dual fluorescent protein biosensors of the type represented by mt-Rosella in cells treated with CCCP has been previously pointed out (Padman *et al.* 2013).

**Discussion**

In this work we have set out to systematically study potential triggers of the mitophagic pathway in neurons by focusing on the respiratory electron transport chain. We have specifically addressed the question of the role of depolarization of mitochondria in activation of mitophagy. The technical approaches we brought to bear on these issues are based on: (i) assessment of mitochondrial respiration using Seahorse technology; (ii) determination of the polarization of mitochondria in live neurons using the reporter TMRM whose accumulation into mitochondria is voltage-dependent; (iii) recruitment of PINK1 to the earlier phase of mitophagic cascade by immunocytochemistry; and (iv) assessment of the transfer of mitochondria into the acidic lysosomal environment during later phases of mitophagy by means of a fluorescent intramitochondrial molecular reporter.

By targeting mitochondria with a series of agents affecting particular respiratory enzyme complexes, we have been able to establish two key findings. First, the loss of $\Delta\Psi_m$, as such, is not a necessary condition for the triggering of neuronal mitophagy. Thus, 3-NP failed to depolarize mitochondria extensively but was an efficient trigger of mitophagy. Second, even where almost complete mitochondrial depolarization can be effected, the subsequent progress of mitophagy may occur sluggishly or not at all. Evidence that depolarization may not be sufficient in itself to trigger mitophagy was obtained by use of AA or KCN, each of which depolarized mitochondria effectively, although with weakened PINK1 recruitment to mitochondria, but no evidence of acidification of mitochondria. By contrast, the cellular response to Rot appeared to support previous findings (Narendra *et al.* 2010), in that this agent caused effective depolarization of mitochondria in neurons followed by a robust mitophagy. The differential effects of focused respiratory chain disruption provide new insights into the complexity of how mitophagy may be triggered in neurons.

Much of the current thinking on PINK1- and Parkin-dependent mitophagy is influenced by the viewpoint that mitochondria that have somehow become inefficient in bioenergetic processes, manifested by loss of $\Delta\Psi_m$, are rendered as suitable targets for mitophagic destruction within the cell. Thus, in experimental mimicking of this concept, especially in non-neuronal or immortalized cell lines, mitochondria subjected to abrupt depolarization by so-called uncoupling agents such as CCCP or FCCP respond by the accumulation of PINK1 on the OMM,

thereby initiating mitophagy via a Parkin-dependent mechanism (Narendra *et al.* 2008, Matsuda *et al.* 2010). Our present results using cultured neurons suggest that the previous approaches applied to perhaps less specialized cell types may have obscured some of the more subtle aspects of mitophagic induction, although having revealed the basic molecular machinery of mitophagy. However, the mechanistic differences leading to differential depolarization of mitochondria by Rot and AA (Fig. 2) are not clear.

Assuming that neurons do retain the basic molecular machinery of PINK1- and Parkin-dependent mitophagy, our observations can be melded into this framework as follows. We postulate that the overall metabolic state of a cell, perhaps over-ridden by metabolic disturbances effected by certain inhibitors, may provide potent influences on the induction of mitophagy. Neurons are differentiated cells with an exquisite reliance on OXPHOS for bioenergetic requirements. By contrast, the non-neuronal or immortalized cell lines used in many previous studies on mitophagy rely much more on glycolytic metabolism than neurons. Indeed, a close link between bioenergetics of cells and mitophagy was demonstrated in a previous study involving HeLa cells. These cells usually display robust mitophagy upon depolarization of $\Delta\Psi_m$ under normal culture conditions (Narendra *et al.* 2008, Narendra *et al.* 2010, Ding *et al.* 2010, Van Laar *et al.* 2011). However, when cells were induced to enter a very substantial dependence on mitochondrial OXPHOS for energy production in preference to glycolysis, mitophagy was remarkably repressed (Van Laar *et al.* 2011). These workers reported that a global application of CCCP to primary cortical neurons failed to show Parkin translocation to mitochondria for initiation of mitophagy. On the contrary, HeLa cells in the same study showed a rapid and robust localization of Parkin to mitochondria (Van Laar *et al.* 2011). Interestingly, when HeLa cells were forced to rely on mitochondrial respiration for energy by blocking glycolysis, translocation of Parkin to depolarized mitochondria was not observed (Van Laar *et al.* 2011). These findings, together with the present work, emphasize how the metabolic profile of cells that have highly developed mitochondrial ATP generation plays a characteristic role in recruiting mitophagy.

In this light, neurons may represent a class of differentiated cells highly dependent upon OXPHOS, in which depolarization of mitochondria may not be a universally effective trigger for mitophagy. The CGCs used here were extensively differentiated to generate abundant neuritic arbors, closely resembling the regular physiological morphology (Benito-Cuesta *et al.* 2017). Moreover, the Seahorse data (Fig. 1) showed the extent to which the untreated neurons presented as oxidative in character. Interestingly in these mature primary neurons subjected to inhibition of mitochondrial OXPHOS complexes I or II, induction of mitophagy was very efficient after blockade of the respiratory chain, although in the latter case little depolarization of mitochondria occurred. This evidence is perhaps suggestive of metabolic disturbance being a potent factor in the triggering of mitophagy in neurons. Inhibition of Complex II by 3-NP would not directly affect the pumping of $H^+$ across the IMM. This agent would disrupt the flow of metabolites in the TCA cycle as its major effect, which would indirectly influence the balance of oxidation and reduction at the level of FAD and NAD coenzymes. The action of Rot in inhibiting Complex I would directly block NAD oxidation as well as leading to reduced translocation of $H^+$ across the IMM (contributing to depolarization). In these neurons, it may the former effect on oxidation-reduction of metabolites that is the key trigger for mitophagy.

In the case of inhibition of Complex III or IV by AA or KCN, respectively, although depolarization occurs the disruption to metabolism may not be the same as for the other inhibitors used. Indeed, earlier studies using

primary neurons have shown not only a loss of $\Delta\Psi_m$, but other factors such as the culture conditions or the presence of antioxidants could influence the triggering of neuronal mitophagy (Van Laar *et al.* 2011, Seibler *et al.* 2011, Cai *et al.* 2012, Joselin *et al.* 2012, Rakovic *et al.* 2013, McCoy *et al.* 2014). The identification of the key metabolites in mitophagic induction remains to be determined.

The role of PINK1 as being universally involved as a trigger for mitophagy may also need reconsideration. Is mitochondrial localization of PINK1 sufficient as a trigger for mitophagy in neurons? Does PINK1 possess additional cellular functions outside PINK1/Parkin-mediated mitophagy upon recruitment to mitochondria? While the role of PINK1 in promoting mitophagy has been a topic of great interest, there is also an additional body of evidence demonstrating a dual role of PINK1 as a suppressor of mitophagy. Specifically, PINK1 has been suggested to reduce the triggering of mitophagy by preserving mitochondrial membrane potential; it binds to Parkin in the cytosol to prevent its translocation to damaged mitochondria (Gegg *et al.* 2009, Morais *et al.* 2014, Steer *et al.* 2015). In this view, it is conceivable that the bioenergetic dysfunction induced by complex III and IV inhibition in this work may have been below the threshold for PINK1 acting as trigger for mitophagy; thus, the turnover of mitochondria may have been suppressed in the experiments reported in this study. Mechanisms underpinning the role of PINK1 as a switch that determines the progression to either PINK1/Parkin-mediated mitophagy, or the upregulation of pro-survival mechanisms and suppression of mitophagy, still remain to be fully elucidated (Liu *et al.* 2011, Murata *et al.* 2011, Dagda *et al.* 2014, Fedorowicz *et al.* 2014). Future work to analyze the translocation of Parkin under these conditions will be important.

In this work, monitoring of late stage of mitophagy was achieved using the dual fluorescence biosensor, mt-Rosella, enabling the observation of mitophagy in various morphologically defined regions of neurons. Ours is the first study to utilize this mitochondrial reporter in mammalian neurons although its successful usage in HeLa cells has been reported (Sargsyan *et al.* 2015). In our study a noteworthy finding was that the most prevalent recruitment of mitophagy in our study took place at the distal ends of the neuritic processes after inhibition of complexes I and II. Recently we successfully employed mt-Rosella to analyze PINK1/Parkin-dependent mitophagy in human primary fibroblasts from control and Parkinsonian patients (Bonello *et al.* 2019). Of course, fibroblasts do not possess the extended distal processes of neurons and here the vesicular labelling predominantly surrounded the nucleus (Bonello *et al.* 2019). There are, however other reports using different reporters of abundant PINK1/Parkin-dependent mitophagy in distal neuronal axons of pluripotent stem cell-derived neurons from PD patients (Hsieh *et al.* 2016) and rodent hippocampal neurons (Ashrafi *et al.* 2014, Maday & Holzbaur 2014). Thus, others have postulated at such distal regions a mechanism involving the continuous generation of autophagosomes associated with local mitophagy of dysfunctional mitochondria, observed in axons and axon tips in primary neuronal cultures (Ashrafi *et al.* 2014, Maday & Holzbaur 2014, Hsieh *et al.* 2016). The recruitment of mitophagy may be more prevalent at the distal ends of the neuritic processes after inhibition of complexes I and II, compared to that in the cell body. Higher resolution analyses of the mitophagy events in the region of the cell body would be required to settle this point, including the use of markers of autophagy. Under physiological conditions, neurons require efficient distribution of mitochondria to distal areas where energy is in high demand, such as synaptic terminals, active growth cones and axonal branches (Morris & Hollenbeck 1993, Ruthel & Hollenbeck 2003); thus, aged and damaged

mitochondria need to be efficiently removed by mitophagy at the distal ends of post-mitotic neurons (Sheng 2014).

Our observations highlight the importance of an appropriate operation of mitochondrial quality control in post-mitotic neurons as mitochondrial function is closely associated with neuronal viability. Dysfunctional aspects of mitochondria have been a major theme in many neurodegenerative diseases. Therefore, understanding the mechanisms of neuronal mitochondrial quality control relevant to mitophagy is of key importance.

**Acknowledgments**

The authors declare no conflict of interest. YSS was in receipt of a scholarship from Australian Postgraduate Award and the University of Melbourne. This work was supported by the National Health and Medical Research Council (Australia) (APP509217), of which PMB was a Research Fellow (APP1020401). PN and RJD were supported by the Australian Research Council. PMB acknowledges support of Operational Infrastructure Scheme from the Victorian Government Department of Business and Innovation. We thank Dr Carlos Rosado and Dr Percy Chu for advice and assistance in this work. The generous provision of the PINK1 antibody by Dr Janetta Culvenor is gratefully acknowledged.

--Human subjects --
Involves human subjects:
If yes: Informed consent & ethics approval achieved:
=> if yes, please ensure that the info "Informed consent was achieved for all subjects, and the experiments were approved by the local ethics committee." is included in the Methods.

ARRIVE guidelines have been followed:
No
=> if it is a Review or Editorial, skip complete sentence => if No, include a statement: "ARRIVE guidelines were not followed for the following reason:
No experiments on live animals were carried out for this study. "
(edit phrasing to form a complete sentence as necessary).
=> if Yes, insert "All experiments were conducted in compliance with the ARRIVE guidelines." unless it is a Review or Editorial

**References**

Ashrafi G., Schlehe J. S., LaVoie M. J. and Schwarz T. L. (2014) Mitophagy of damaged mitochondria occurs locally in distal neuronal axons and requires PINK1 and Parkin. J Cell Biol, **206,** 655-670.

Ashrafi G. and Schwarz T. L. (2013) The pathways of mitophagy for quality control and clearance of mitochondria. Cell Death Differ, **20,** 31-42.

Baker M. J., Palmer C. S. and Stojanovski D. (2014) Mitochondrial protein quality control in health and disease. Br J Pharmacol, **171,** 1870-1889.

Beal M. F. (2005) Mitochondria take center stage in aging and neurodegeneration. Ann of Neurol, **58,** 495-505.

Beart P. M., Lim M. L., Chen B., Diwakarla S., Mercer L. D., Cheung N. S. and Nagley P. (2007) Hierarchical recruitment by AMPA but not staurosporine of pro-apoptotic mitochondrial signaling in cultured cortical neurons: evidence for caspase-dependent/independent cross-talk. J Neurochem, **103,** 2408-2427.

Benito-Cuesta I., Diez H., Ordonez L. and Wandosell F. (2017) Assessment of autophagy in neurons and brain tissue. Cells, **6**, 25.

Bingol B. and Sheng M. (2016) Mechanisms of mitophagy: PINK1, Parkin, USP30 and beyond. Free Radic Biol Med, **100,** 210-222.

Bonello F., Hassoun S. M., Mouton-Liger F., Shin Y. S., Muscat A., Tesson C., Lesage S., Beart P. M., Brice A., Krupp J., Corvol J. C. and Corti O. (2019) LRRK2 impairs PINK1/Parkin-dependent mitophagy via its kinase activity: pathologic insights into Parkinson's disease. Hum Mol Genet (HMG-2018-D-00751) accepted 1st January 2019.

Cai Q., Zakaria H. M., Simone A. and Sheng Z. H. (2012) Spatial parkin translocation and degradation of damaged mitochondria via mitophagy in live cortical neurons. Curr Biol, **22,** 545-552.

Chaturvedi R. K. and Beal M. F. (2013) Mitochondria targeted therapeutic approaches in Parkinson's and Huntington's diseases. Mole Cell Neurosci, **55,** 101-114.

Chen H. and Chan D. C. (2009) Mitochondrial dynamics--fusion, fission, movement, and mitophagy--in neurodegenerative diseases. Hum Mol Genet, **18,** R169-176.

Cheung N. S., Carroll F. Y., Larm J. A., Beart P. M. and Giardina S. F. (1998) Kainate-induced apoptosis correlates with c-Jun activation in cultured cerebellar granule cells. J Neurosci Res, **52,** 69-82.

Dagda R. K., Pien I., Wang R., Zhu J., Wang K. Z., Callio J., Banerjee T. D., Dagda R. Y. and Chu C. T. (2014) Beyond the mitochondrion: cytosolic PINK1 remodels dendrites through protein kinase A. J Neurochem, **128,** 864-877.

Degli Esposti M. (1998) Inhibitors of NADH-ubiquinone reductase: an overview. Biochim Biophys Acta, **1364,** 222-235.

Ding W. X., Ni H. M., Li M., Liao Y., Chen X., Stolz D. B., Dorn G. W., 2nd and Yin X. M. (2010) Nix is critical to two distinct phases of mitophagy, reactive oxygen species-mediated autophagy induction and Parkin-ubiquitin-p62-mediated mitochondrial priming. J Biol Chem, **285,** 27879-27890.

Diwakarla S., Nagley P., Hughes M. L., Chen B. and Beart P. M. (2009) Differential insult-dependent recruitment of the intrinsic mitochondrial pathway during neuronal programmed cell death. Cell Mol Life Sci, **66,** 156-172.

Elmore S. P., Qian T., Grissom S. F. and Lemasters J. J. (2001) The mitochondrial permeability transition initiates autophagy in rat hepatocytes. FASEB J, **15,** 2286-2287.

Fedorowicz M. A., de Vries-Schneider R. L., Rub C., Becker D., Huang Y., Zhou C., Alessi Wolken D. M., Voos W., Liu Y. and Przedborski S. (2014) Cytosolic cleaved PINK1 represses Parkin translocation to mitochondria and mitophagy. EMBO Rep, **15,** 86-93.

Gegg M. E., Cooper J. M., Schapira A. H. and Taanman J. W. (2009) Silencing of PINK1 expression affects mitochondrial DNA and oxidative phosphorylation in dopaminergic cells. PLoS One, **4,** e4756.

Geisler S., Holmstrom K. M., Skujat D., Fiesel F. C., Rothfuss O. C., Kahle P. J. and Springer W. (2010) PINK1/Parkin-mediated mitophagy is dependent on VDAC1 and p62/SQSTM1. Nat Cell Biol, **12,** 119-131.

George S., Mok S. S., Nurjono M., Ayton S., Finkelstein D. I., Masters C. L., Li Q. X. and Culvenor J. G. (2010) alpha-Synuclein transgenic mice reveal compensatory increases in Parkinson's disease-associated proteins DJ-1 and parkin and have enhanced alpha-synuclein and PINK1 levels after rotenone treatment. J Mol Neurosci, **42,** 243-254.

Giardina S. F., Cheung N. S., Reid M. T. and Beart P. M. (1998) Kainate-induced apoptosis in cultured murine cerebellar granule cells elevates expression of the cell cycle gene cyclin D1. J Neurochem, **71,** 1325-1328.

Golpich M., Amini E., Mohamed Z., Ali R. A., Ibrahim N. M. and Ahmadiani A. (2017) Mitochondrial dysfunction and biogenesis in neurodegenerative diseases: Pathogenesis and treatment. CNS Neurosci Ther, **23,** 5-22.

Higgins G. C., Beart P. M. and Nagley P. (2009) Oxidative stress triggers neuronal caspase-independent death: endonuclease G involvement in programmed cell death-type III. Cell Mol Life Sci, **66,** 2773-2787.

Hsieh C. H., Shaltouki A., Gonzalez A. E., Bettencourt da Cruz A., Burbulla L. F., St Lawrence E., Schule B., Krainc D., Palmer T. D. and Wang X. (2016) Functional impairment in Miro degradation and mitophagy is a shared feature in familial and sporadic Parkinson's disease. Cell Stem Cell, **19,** 709-724.

Huang L. S., Cobessi D., Tung E. Y. and Berry E. A. (2005) Binding of the respiratory chain inhibitor antimycin to the mitochondrial bc1 complex: a new crystal structure reveals an altered intramolecular hydrogen-bonding pattern. J Mol Biol, **351,** 573-597.

Huang L. S., Sun G., Cobessi D., Wang A. C., Shen J. T., Tung E. Y., Anderson V. E. and Berry E. A. (2006) 3-nitropropionic acid is a suicide inhibitor of mitochondrial respiration that, upon oxidation by complex II, forms a covalent adduct with a catalytic base arginine in the active site of the enzyme. J Biol Chem, **281,** 5965-5972.

Jin S. M., Lazarou M., Wang C., Kane L. A., Narendra D. P. and Youle R. J. (2010) Mitochondrial membrane potential regulates PINK1 import and proteolytic destabilization by PARL. J Cell Biol, **191,** 933-942.

Joselin A. P., Hewitt S. J., Callaghan S. M., Kim R. H., Chung Y. H., Mak T. W., Shen J., Slack R. S. and Park D. S. (2012) ROS-dependent regulation of Parkin and DJ-1 localization during oxidative stress in neurons. Hum Mol Genet, **21,** 4888-4903.

Kane L. A., Lazarou M., Fogel A. I., Li Y., Yamano K., Sarraf S. A., Banerjee S. and Youle R. J. (2014) PINK1 phosphorylates ubiquitin to activate Parkin E3 ubiquitin ligase activity. J Cell Biol, **205,** 143-153.

Kanki T. and Klionsky D. J. (2008) Mitophagy in yeast occurs through a selective mechanism. J Biol Chem, **283,** 32386-32393.

Kann O. and Kovacs R. (2007) Mitochondria and neuronal activity. Am J Physiol Cell Physiol, **292,** C641-657.

Kim I., Rodriguez-Enriquez S. and Lemasters J. J. (2007) Selective degradation of mitochondria by mitophagy. Arch Biochem Biophys, **462,** 245-253.

Kondapalli C., Kazlauskaite A., Zhang N., Woodroof H. I., Campbell D. G., Gourlay R., Burchell L., Walden H., Macartney T. J., Deak M., Knebel A., Alessi D. R. and Muqit M. M. (2012) PINK1 is activated by mitochondrial membrane potential depolarization and stimulates Parkin E3 ligase activity by phosphorylating Serine 65. Open Biol, **2,** 120080.

Lazarou M., Sliter D. A., Kane L. A., Sarraf S. A., Wang C., Burman J. L., Sideris D. P., Fogel A. I. and Youle R. J. (2015) The ubiquitin kinase PINK1 recruits autophagy receptors to induce mitophagy. Nature, **524,** 309-314.

Lemasters J. J. (2005) Selective mitochondrial autophagy, or mitophagy, as a targeted defense against oxidative stress, mitochondrial dysfunction, and aging. Rejuvenation Res, **8,** 3-5.

Lim M. L., Mercer L. D., Nagley P. and Beart P. M. (2007) Rotenone and MPP+ preferentially redistribute apoptosis-inducing factor in apoptotic dopamine neurons. Neuroreport, **18,** 307-312.

Lim M. L., Minamikawa T. and Nagley P. (2001) The protonophore CCCP induces mitochondrial permeability transition without cytochrome c release in human osteosarcoma cells. FEBS Lett, **503,** 69-74.

Liu W., Acin-Perez R., Geghman K. D., Manfredi G., Lu B. and Li C. (2011) Pink1 regulates the oxidative phosphorylation machinery via mitochondrial fission. Proc Natl Acad Sci U S A, **108,** 12920-12924.

Maday S. and Holzbaur E. L. (2014) Autophagosome biogenesis in primary neurons follows an ordered and spatially regulated pathway. Dev Cell, **30,** 71-85.

Matsuda N., Sato S., Shiba K., Okatsu K., Saisho K., Gautier C. A., Sou Y. S., Saiki S., Kawajiri S., Sato F., Kimura M., Komatsu M., Hattori N. and Tanaka K. (2010) PINK1 stabilized by mitochondrial depolarization recruits Parkin to damaged mitochondria and activates latent Parkin for mitophagy. J Cell Biol, **189,** 211-221.

McCoy M. K., Kaganovich A., Rudenko I. N., Ding J. and Cookson M. R. (2014) Hexokinase activity is required for recruitment of parkin to depolarized mitochondria. Hum Mol Genet, **23,** 145-156.

Mercer L. D., Higgins G. C., Lau C. L., Lawrence A. J. and Beart P. M. (2017) MDMA-induced neurotoxicity of serotonin neurons involves autophagy and rilmenidine is protective against its pathobiology. Neurochem Int, **105,** 80-90.

Mercer L. D., Kelly B. L., Horne M. K. and Beart P. M. (2005) Dietary polyphenols protect dopamine neurons from oxidative insults and apoptosis: investigations in primary rat mesencephalic cultures. Biochem Pharmacol, **69,** 339-345.

Mijaljica D., Prescott M. and Devenish R. J. (2011) A Fluorescence microscopy assay for monitoring mitophagy in the yeast saccharomyces cerevisiae. JoVE**,** e2779.

Minamikawa T., Williams D. A., Bowser D. N. and Nagley P. (1999) Mitochondrial permeability transition and swelling can occur reversibly without inducing cell death in intact human cells. Exp Cell Res, **246,** 26-37.

Moldrich R. X., Giardina S. F. and Beart P. M. (2001) Group II mGlu receptor agonists fail to protect against various neurotoxic insults induced in murine cortical, striatal and cerebellar granular pure neuronal cultures. Neuropharmacology, **41,** 19-31.

Morais V. A., Haddad D., Craessaerts K., De Bock P. J., Swerts J., Vilain S., Aerts L., Overbergh L., Grunewald A., Seibler P., Klein C., Gevaert K., Verstreken P. and De Strooper B. (2014) PINK1 loss-of-function mutations affect mitochondrial complex I activity via NdufA10 ubiquinone uncoupling. Science, **344,** 203-207.

Morris R. L. and Hollenbeck P. J. (1993) The regulation of bidirectional mitochondrial transport is coordinated with axonal outgrowth. J Cell Sci, **104,** 917-927.

Murata H., Sakaguchi M., Kataoka K. and Huh N. H. (2011) Multiple functions of PINK1 at different intracellular locations: beyond neurodegenerative diseases. Cell Cycle, **10,** 1518-1519.

Narendra D., Tanaka A., Suen D. F. and Youle R. J. (2008) Parkin is recruited selectively to impaired mitochondria and promotes their autophagy. J Cell Biol, **183,** 795-803.

Narendra D. P., Jin S. M., Tanaka A., Suen D. F., Gautier C. A., Shen J., Cookson M. R. and Youle R. J. (2010) PINK1 is selectively stabilized on impaired mitochondria to activate Parkin. PLoS Biol, **8,** e1000298.

Okatsu K., Oka T., Iguchi M., Imamura K., Kosako H., Tani N., Kimura M., Go E., Koyano F., Funayama M., Shiba-Fukushima K., Sato S., Shimizu H., Fukunaga Y., Taniguchi H., Komatsu M., Hattori N., Mihara K., Tanaka K. and Matsuda N. (2012) PINK1 autophosphorylation upon membrane potential dissipation is essential for Parkin recruitment to damaged mitochondria. Nat Commun, **3,** 1016.

Okatsu K., Uno M., Koyano F., Go E., Kimura M., Oka T., Tanaka K. and Matsuda N. (2013) A dimeric PINK1-containing complex on depolarized mitochondria stimulates Parkin recruitment. J Biol Chem, **288,** 36372-36384.

Ordureau A., Sarraf S. A., Duda D. M., Heo J. M., Jedrychowski M. P., Sviderskiy V. O., Olszewski J. L., Koerber J. T., Xie T., Beausoleil S. A., Wells J. A., Gygi S. P., Schulman B. A. and Harper J. W. (2014) Quantitative proteomics reveal a feedforward mechanism for mitochondrial PARKIN translocation and ubiquitin chain synthesis. Mol Cell, **56,** 360-375.

Padman B. S., Bach M., Lucarelli G., Prescott M. and Ramm G. (2013) The protonophore CCCP interferes with lysosomal degradation of autophagic cargo in yeast and mammalian cells. Autophagy, **9,** 1862-1875.

Priault M., Salin B., Schaeffer J., Vallette F. M., di Rago J. P. and Martinou J. C. (2005) Impairing the bioenergetic status and the biogenesis of mitochondria triggers mitophagy in yeast. Cell Death Differ, **12,** 1613-1621.

Rakovic A., Shurkewitsch K., Seibler P., Grunewald A., Zanon A., Hagenah J., Krainc D. and Klein C. (2013) Phosphatase and tensin homolog (PTEN)-induced putative kinase 1 (PINK1)-dependent ubiquitination of endogenous Parkin attenuates mitophagy: study in human primary fibroblasts and induced pluripotent stem cell-derived neurons. J Biol Chem, **288,** 2223-2237.

Rodriguez-Enriquez S., He L. and Lemasters J. J. (2004) Role of mitochondrial permeability transition pores in mitochondrial autophagy. Int J Biochem Cell Biol, **36,** 2463-2472.

Rosado C. J., Mijaljica D., Hatzinisiriou I., Prescott M. and Devenish R. J. (2008) Rosella: a fluorescent pH-biosensor for reporting vacuolar turnover of cytosol and organelles in yeast. Autophagy, **4,** 205-213.

Ruthel G. and Hollenbeck P. J. (2003) Response of mitochondrial traffic to axon determination and differential branch growth. J Neurosci, **23,** 8618-8624.

Ryall J. G. (2017) Simultaneous Measurement of mitochondrial and glycolytic activity in quiescent muscle stem cells. Methods Mol Biol, **1556,** 245-253.

Sargsyan A., Cai J., Fandino L. B., Labasky M. E., Forostyan T., Colosimo L. K., Thompson S. J. and Graham T. E. (2015) Rapid parallel measurements of macroautophagy and mitophagy in mammalian cells using a single fluorescent biosensor. Sci Rep, **5,** 12397.

Sarraf S. A., Raman M., Guarani-Pereira V., Sowa M. E., Huttlin E. L., Gygi S. P. and Harper J. W. (2013) Landscape of the PARKIN-dependent ubiquitylome in response to mitochondrial depolarization. Nature, **496,** 372-376.

Scheffler I. E. (2011) *Mitochondria*. 2nd ed. Wiley.

Seibler P., Graziotto J., Jeong H., Simunovic F., Klein C. and Krainc D. (2011) Mitochondrial Parkin recruitment is impaired in neurons derived from mutant PINK1 induced pluripotent stem cells. J Neurosci, **31,** 5970-5976.

Sekine S. and Youle R. J. (2018) PINK1 import regulation; a fine system to convey mitochondrial stress to the cytosol. BMC Biol, **16,** 2.

Sheng Z. H. (2014) Mitochondrial trafficking and anchoring in neurons: New insight and implications. J Cell Biol, **204,** 1087-1098.

Smith D. J., Ng H., Kluck R. M. and Nagley P. (2008) The mitochondrial gateway to cell death. IUBMB Life, **60,** 383-389.

Steer E. K., Dail M. K. and Chu C. T. (2015) Beyond mitophagy: cytosolic PINK1 as a messenger of mitochondrial health. Antioxid Redox Signal, **22,** 1047-1059.

Twig G., Elorza A., Molina A. J., Mohamed H., Wikstrom J. D., Walzer G., Stiles L., Haigh S. E., Katz S., Las G., Alroy J., Wu M., Py B. F., Yuan J., Deeney J. T., Corkey B. E. and Shirihai O. S. (2008) Fission and selective fusion govern mitochondrial segregation and elimination by autophagy. EMBO J, **27,** 433-446.

Van Laar V. S., Arnold B., Cassady S. J., Chu C. T., Burton E. A. and Berman S. B. (2011) Bioenergetics of neurons inhibit the translocation response of Parkin following rapid mitochondrial depolarization. Hum Mol Genet, **20,** 927-940.

Van Laar V. S., Roy N., Liu A., Rajprohat S., Arnold B., Dukes A. A., Holbein C. D. and Berman S. B. (2015) Glutamate excitotoxicity in neurons triggers mitochondrial and endoplasmic reticulum accumulation of Parkin, and, in the presence of N-acetyl cysteine, mitophagy. Neurobiol Dis, **74,** 180-193.

Vives-Bauza C., Zhou C., Huang Y., Cui M., de Vries R. L., Kim J., May J., Tocilescu M. A., Liu W., Ko H. S., Magrane J., Moore D. J., Dawson V. L., Grailhe R., Dawson T. M., Li C., Tieu K. and Przedborski S. (2010) PINK1-dependent recruitment of Parkin to mitochondria in mitophagy. Proc Natl Acad Sci U S A, **107,** 378-383.

Way J. L. (1984) Cyanide intoxication and its mechanism of antagonism. Annu Rev Pharmacol Toxicol, **24,** 451-481.

Youle R. J. and Narendra D. P. (2011) Mechanisms of mitophagy. Nature Reviews Molecular Cell Biology, **12,** 9-14.

**Table 1** Effective concentrations of mitochondrial respiratory complex inhibitors

| Drug | Site of action | $IC_{50}$±SEM | Concentrations (low, high) |
|---|---|---|---|
| Rotenone (Rot) | Complex I | 100 ± 17 nM | 10 nM, 30 nM |
| 3-Nitropropionic acid (3-NP) | Complex II | 78 ± 33 µM | 100 µM, 300 µM |
| Antimycin A (AA) | Complex III | 42 ± 1.3 nM | 10 nM, 30 nM |
| Potassium cyanide (KCN) | Complex IV | 1.2 ± 0.5 mM | 100 µM, 300 µM |

CGCs were treated with drugs to establish the $IC_{50}$ using the MTT test (Supplementary Fig. 1). Two concentrations of each drug were chosen for optimal inhibition (Way 1984, Degli Esposti 1998, Huang *et al.* 2005, Huang *et al.* 2006) of the target respiratory complex (see text). Values are the mean +/- SEM from n = 3 - 4 independent experiments employing 4 replicate determinations

**LEGENDS TO FIGURES**

**Fig. 1** XF Metabolic PhenoGrams. The bioenergetic state of CGCs was determined from data obtained using a Seahorse Extracellular Flux (XF) Analyzer XF24 for the oxygen consumption rate (OCR) and extracellular acidification rate (ECAR). For each drug tested an XF PhenoGram of ECAR versus OCR was constructed (raw data in Supplementary Fig. 3) to determine the metabolic profile of cells in their basal state. Panel (a) shows the assigned metabolic state for four ranges of ECAR/OCR values, based on arbitrary delimitation into four quadrants in order to distinguish cells in various metabolic states after treatment (see text). XF metabolic PhenoGrams for four drug treatment regimens are presented as follows: (b) lower drug concentrations after 4 h (n = 4 Rot 10 nM, n = 5 3-NP 100 µM, n = 4 AA 10 nM, n = 4 KCN 100 µM); (c) higher drug concentrations after 4 h (n = 5 Rot 30 nM, n = 5 3-NP 300 µM, n = 5 AA 30 nM, n = 3 KCN 300 µM); (d) lower drug concentrations after 24 h (n = 5 Rot 10 nM, n = 5 3-NP 100 µM, n = 5 AA 10 nM, n = 5 KCN 100 µM); (e) higher drug concentrations after 24 h (n = 5 Rot 30 nM, n = 4 3-NP 300 µM, n = 3 AA 30 nM, n = 3 KCN 300 µM). Data are compiled as mean ± SEM, n = number of replicate wells, from a single treated culture.

**Fig. 2** Depolarization of mitochondria in live cells measured by TMRM fluorescence. (a) Neurons were pre-loaded with TMRM and fluorescence was monitored by confocal live cell imaging at the various times indicated, after administration of each drug. Brightfield view (BF) was simultaneously captured to visualize the total number of cells within the same field; images only shown here for 4 h treatments. Scale bar = 20 µm. (b) Quantification of intracellular TMRM fluorescence. Data are expressed as percentage of control (designated as having 100% fluorescence). All values have been corrected for residual TMRM fluorescence after CCCP treatment. 150-250 cells were counted per treatment at each time point; values are mean ± SEM of 5 independent experiments. Symbols indicate significant loss of TMRM fluorescence at the indicated time of treatment relative to control (* $P < 0.05$; # $P < 0.001$; ## $P < 0.0001$; compared to control by repeated measures two-way ANOVA, followed by Bonferroni's *post hoc* test)

**Fig. 3** Immunocytochemical analysis of PINK1 distribution in neurons. (a) Antibody specific for PINK1 was used to stain neurons immunocytochemically 4 h after drug treatment. Cells were counterstained with Hoechst 33342 to indicate both location and morphology of nuclei. Yellow arrows indicate neurons displaying diffuse distribution of PINK1 fluorescence; white arrows indicate neurons displaying PINK1-specific fluorescence in aggregated morphology (but excluded from the nuclei); red arrows indicate condensed or fragmented nuclei of cells, corresponding to cells showing very weak staining for PINK1. Scale bar = 20 μm. (b) Enlarged images of CGCs from panel A, either untreated (upper row) or treated with 3-NP (lower row). Di indicates diffuse morphology of featured cell; Ag indicates aggregated morphology of two featured cells. Scale bar = 10 μm. Quantitative analysis of PINK1 fluorescence distribution: (c) Rot-treated and 3-NP-treated populations each after 4 h; (d) AA-treated and KCN-treated populations each after 4 h. Neurons were assigned into three distinct morphological populations: diffuse PINK1, aggregated PINK1, and dead cells (as defined above). For each drug treatment (or untreated control), the cell counts were used to quantify each sub-population, expressed as a percentage of the total population of cells counted (total 250-500 cells were counted in each experimental condition) carried out on duplicate wells. Data represent the mean ± SEM of two such independent experiments. Symbols indicate significant differences in distribution of PINK1 relative to control (# $P < 0.0001$, compared to control by two-way ANOVA, followed by Bonferroni's *post hoc* test)

**Fig. 4** Ratiometric fluorescence analysis of live cells expressing mt-Rosella biosensor to monitor acidification of neuronal mitochondria. (a) Representative fields of microscopic images in red channel (DsRed.T4) and green channel (pHluorin). Neurons were transiently transfected with mt-Rosella followed by 24 h exposure to drugs. The pH-insensitive DsRed.T4 fluorescence provided information about the position of mitochondria within the cell while the quenching of pH-sensitive pHluorin fluorescence showed mitochondria in an acidic environment. Scale bar = 40 μm. (b) Green/red fluorescence ratios of regions within neuronal processes (but excluding the cell body) after drug-treatment for 24 h, normalized to the control green/red ratio measured for untreated cells, defined as 100%. Data for CCCP, indicating increased green/red ratios, are discussed in the text. Data represent mean ± SEM of ratios for n = 17-43 cells per condition from two independent experiments. * $P < 0.05$, based on unpaired *t*-test

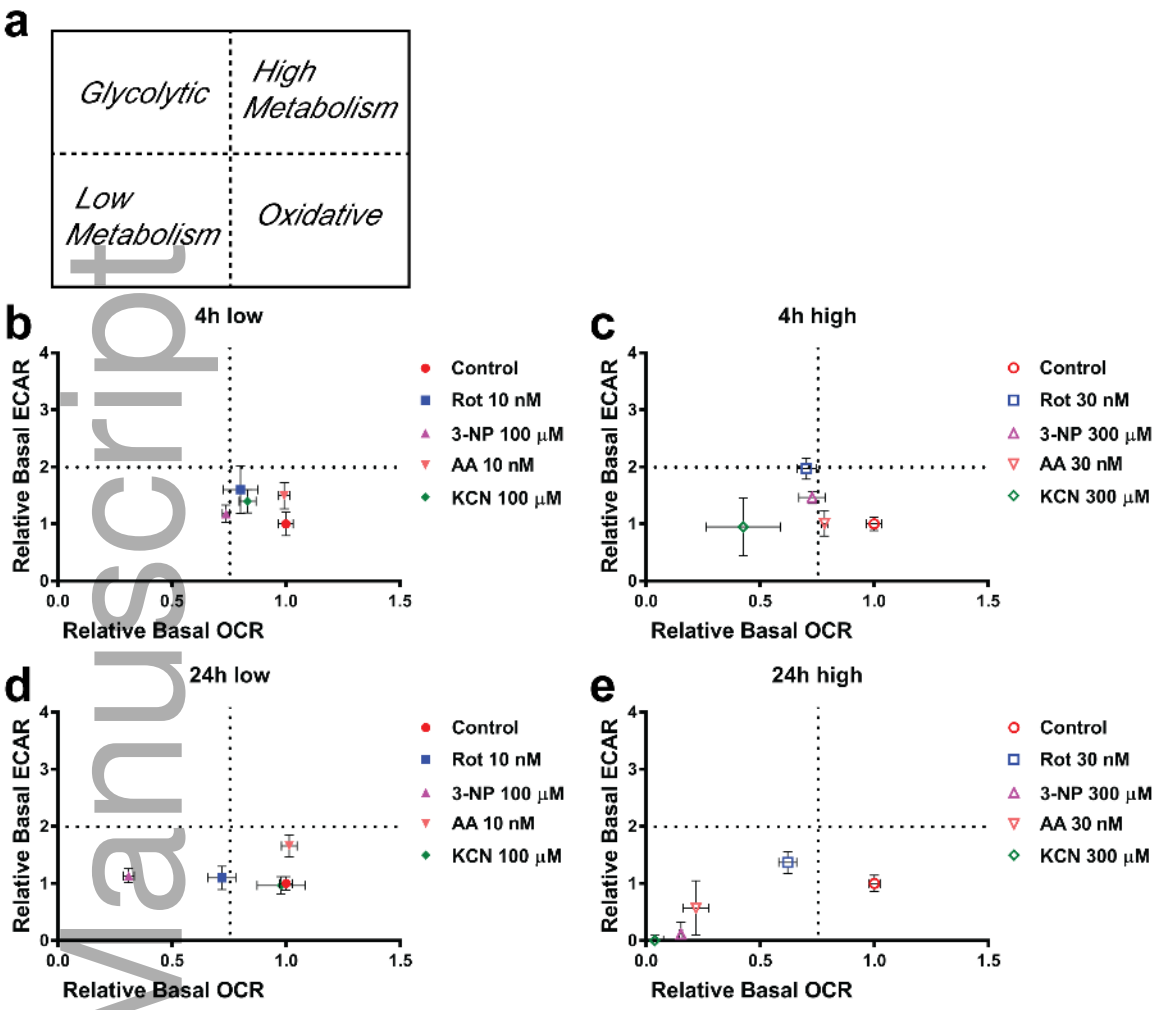


jnc_14667_f1.tif

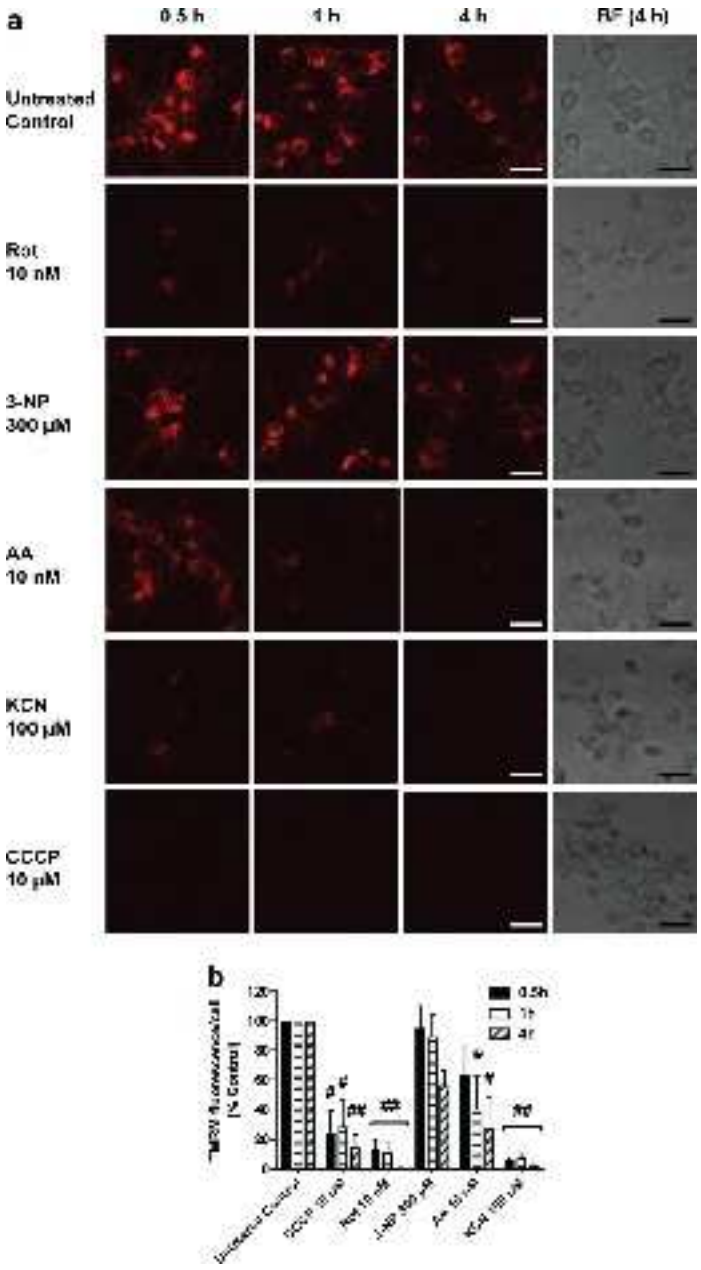


jnc_14667_f2.tif

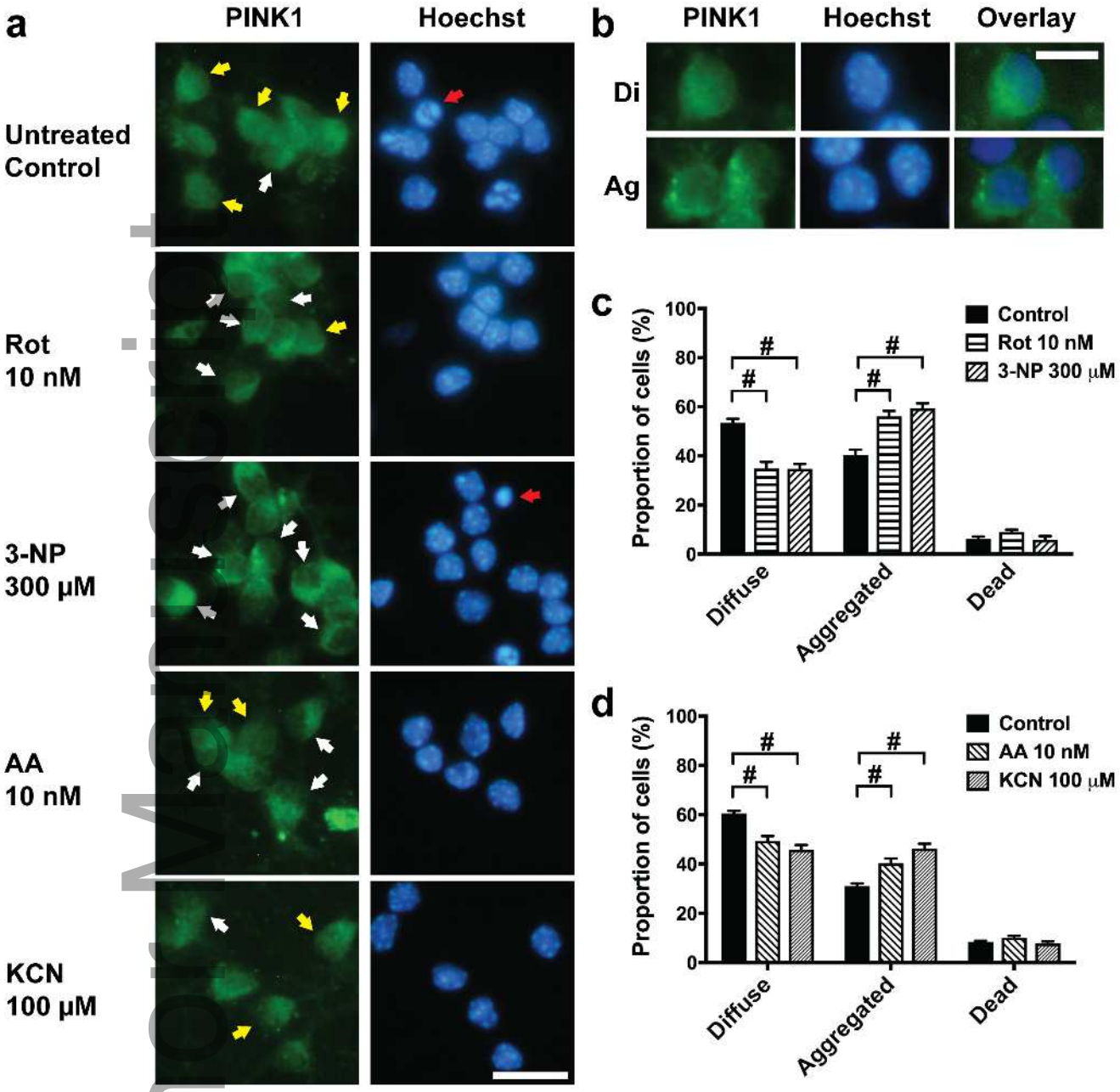


jnc_14667_f3.tif

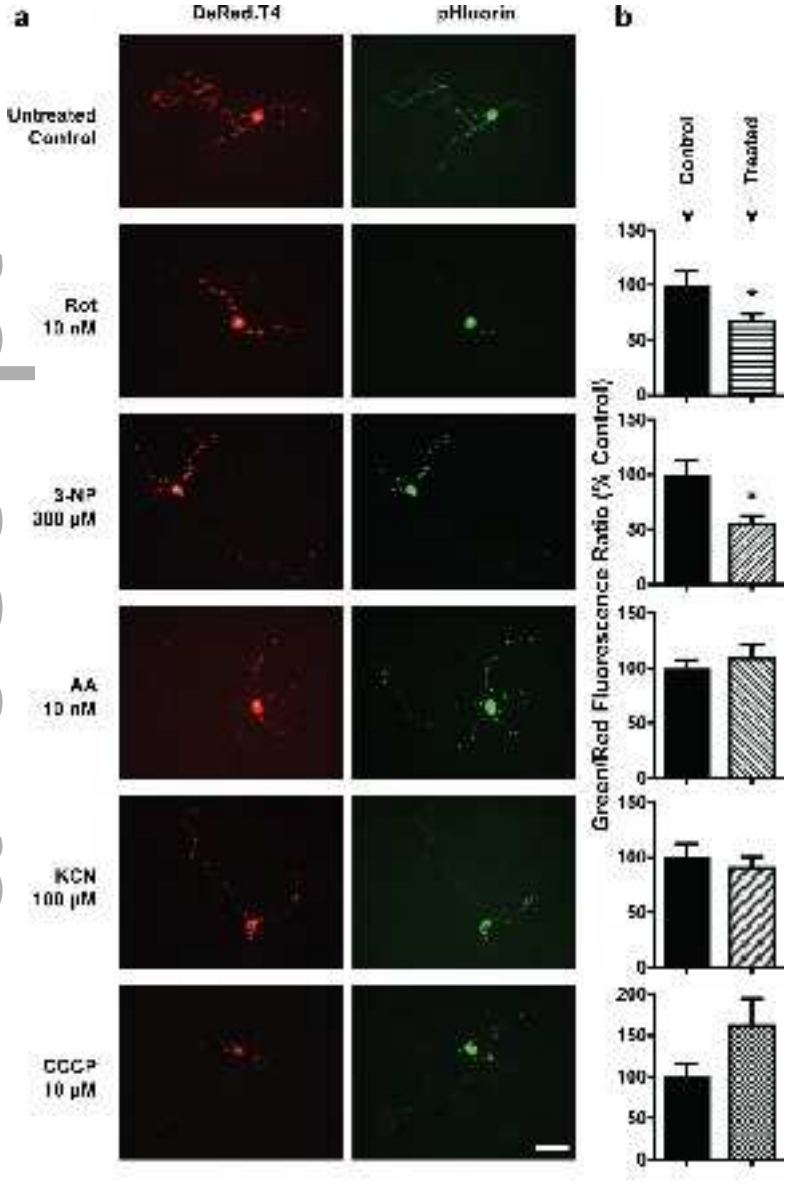


jnc_14667_f4.tif